Mamba Only Glances Once (MOGO): A Lightweight Framework for Efficient Video Action Detection

Yunqing Liu[1], **Nan Zhang**[1], **Fangjun Wang**[1], **Kengo Murata**[2], **Takuma Yamamoto**[2], **Osafumi Nakayama**[2], **Genta Suzuki**[2], **Zhiming Tan**[1*]
[1]Fujitsu R&D Center [2]Fujitsu Research Japan

Abstract

Mamba, a lightweight sequence modeling framework offering near-linear complexity, presents a promising alternative to Transformers. In this work, we introduce MOGO (Mamba Only Glances Once), an end-to-end framework for efficient video action detection built entirely on the Mamba architecture. In MOGO, our newly designed Mamba-based decoder can even use just one Mamba layer to effectively perform action detection. It uses neither Transformer structures nor RCNN-like methods for proposal detection. Our framework introduces two key innovations. First, we propose a pure Mamba-based encoder-decoder architecture. The encoder processes cross-frame video information, while the decoder incorporates two novel Mamba-based structures that leverage Mamba's intrinsic capabilities to detect actions. Theoretical analysis and ablation experiments confirm their synergy and the necessity of each structure. Second, we design a video token construction mechanism to improve the model's performance. The token importance block can ensure that the retained token information is highly relevant to the predicted targets. These two innovations make MOGO both efficient and accurate, as demonstrated on the JHMDB and UCF101-24 benchmark datasets. Compared to SOTA action detection methods, MOGO achieves superior performance in terms of GFLOPs, model parameters, and inference speed (latency) with comparable detection precision. Additionally, it requires significantly less GPU memory than some SOTA token reconstruction methods. Code is available at https://github.com/YunqingLiu-ML/MOGO.

1 Introduction

The goal of video action detection is to localize and classify actions within video sequences, requiring models to capture spatiotemporal dependencies. Recently, Sia and Rawat [1] address this by introducing a lightweight encoder-only model for open-vocabulary detection. Other advancements in this field, such as DETR [2] and TubeR [3], have relied on Transformer-based architectures. These models leverage the attention mechanism to model long-range dependencies across video frames, achieving SOTA performance in capturing temporal context and action semantics. However, the self-attention mechanism incurs quadratic computational complexity with respect to sequence length, making it computationally expensive for long video sequences. For instance, the methods proposed in [4] and [5] achieved significant performance improvements but are reported to have relatively high GFLOPs. This inefficiency makes such models less practical for resource-constrained environments.

The Mamba framework [6] emerges as a promising alternative to Transformers. Unlike the attention-based paradigm, Mamba employs state-space modeling to achieve near-linear complexity, offering a scalable solution for processing spatiotemporal data. Recent adoptions, such as VideoMamba [7] for video classification and MS-Temba [8] for temporal action localization, demonstrate Mamba's

*Corresponding author: zhmtan@fujitsu.com.

39th Conference on Neural Information Processing Systems (NeurIPS 2025).

efficiency in handling sequential data. However, its potential remains underexplored in the context of video action detection.

To develop an efficient and effective framework for video action detection, we proposed a purely Mamba-based framework. The motivation of our design is detailed in Figure 1. The Transformer depends on self-attention and cross attention to capture the dependency relationships. In contrast, Mamba utilizes linear transformations to project queries into target spaces and employs selective copying to efficiently model cross-sequence information. Building on this, we propose MOGO (Mamba Only Glances Once), an end-to-end framework for efficient video action detection. Unlike SOTA methods that incorporate external structures such as RCNN for region proposals [4] or Transformer components like ViT [9], MOGO eliminates the need for these additional modules. Our framework introduces two key innovations:

(1) Pure Mamba-based Architecture. Our designed decoder processes learnable queries and video information tokens through a streamlined pipeline of EQ-Mamba, QVI-Mamba, and an FFN as shown in Figure 2. Ablation studies confirm the synergistic necessity of each module.

(2) Video Token Construction Mechanism. As shown in Figure 3, this module computes importance scores for encoder tokens across spatiotemporal frames. Coupled with an target-guided loss function, this mechanism reduces redundancy and enhances token relevance, further boosting efficiency.

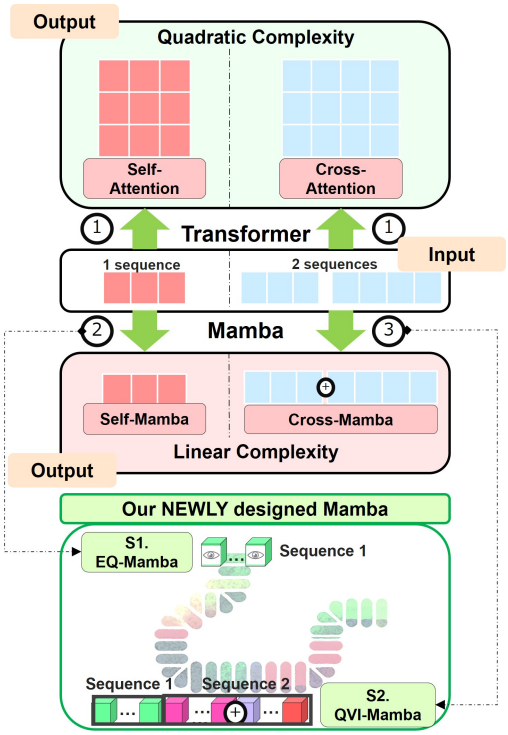

Figure 1: **Motivation of MOGO.** Comparison between Transformer and Mamba complexity inspires our framework design. By *Mamba-izing* the Transformer's (1) attention architecture, our framework enables (2) linear transformation for single-sequence modeling and (3) selective copying mechanism for cross-sequence modeling.

The whole method's main strengths are computational efficiency and a token-importance block, as demonstrated on the JHMDB [10] and UCF101-24 [11] benchmark datasets. Compared to SOTA action detection methods, MOGO achieves superior performance in terms of GFLOPs, model parameters, and inference speed (latency) with comparable detection precision. Additionally, it requires significantly less GPU memory than some SOTA token reconstruction methods.

2 Method

2.1 Overall MOGO Architecture

Our proposed MOGO framework introduces an end-to-end action detection pipeline built entirely on a Mamba-based architecture, as illustrated in Figure 2. Specifically, it detects actions on a designated keyframe within a short video clip while using the remaining frames as temporal context. Because predictions are made on a single keyframe, some non-keyframe tokens may be redundant or weakly informative, which motivates selective token retention and importance modeling, as illustrated in Figure 3. Unlike SOTA methods that incorporate external structures such as RCNN for region proposals [4] or Transformer components like ViT [9], MOGO leverages only Mamba's inherent capabilities, with a primary goal of minimizing computational overhead while maintaining robust detection performance. The MOGO architecture comprises several key components, and the main elements include: Mamba encoder, Mamba decoder, token importance module, and loss function.

2.2 Pure Mamba-based Architecture

Our proposed method adopts an end-to-end purely Mamba-based architecture as shown in Table 1:

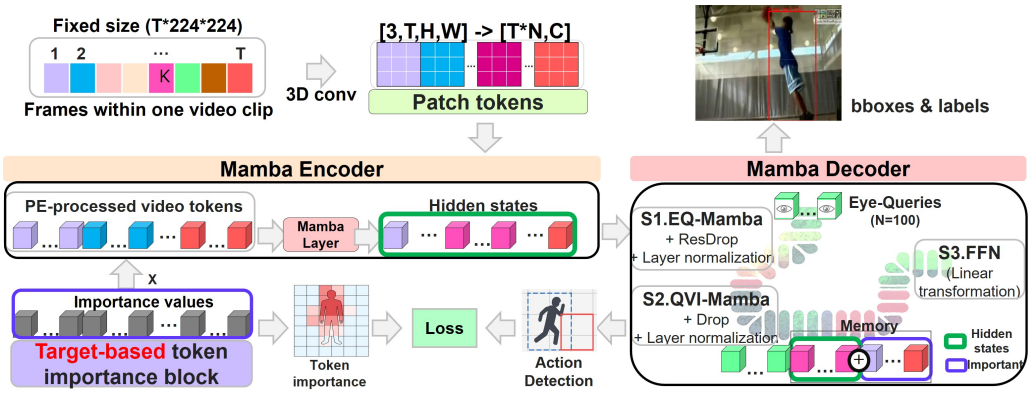

Figure 2: **Overview of the proposed structure.** The encoder processes PE-embedded video tokens through Mamba layers, accompanied by a target-based token importance block that highlights informative regions for action detection. The decoder then operates on two Mamba-based modules followed by a linear layer. Illustration corresponds to batch size = 1. (EQ-Mamba: Eye Query-based Mamba, QVI-Mamba: Query-Video Information-fused Mamba, PE: Positional Embedding, ResDrop: Residual connection with Dropout, Drop: Dropout, K: Key frame.)

Encoder. Leveraging the pretrained models [7], our encoder is designed to extract comprehensive feature maps from input video frames. Following the patch embedding, which transforms the input clip into a sequence of patches, we incorporate spatial positional embeddings and temporal positional embeddings to model inter-frame dependencies across the video sequence. Then we incorporate a bidirectional Mamba setup. The encoder comprises l_e layers, which is evaluated through ablation studies in Section 3.4.

Table 1: **Tensor shape flow across the MOGO architecture.** M contains keyframe tokens and important non-keyframe tokens.

Stage	Tensor	Shape / Description
Input	x	$[B, 3, T, H, W]$
Patch Embedding	Conv3D(x)	$[B, C, T, H', W']$, where $C =$ embed_dim
Flatten and Rearrange	x	$[B, T{\cdot}N, C]$, $N = H' \times W'$
Add Positional Embedding	+PE, +TPE	$[B, T{\cdot}N, C]$
Token Importance Block	MLP(x)	$[B, T{\cdot}N, 1]$
Apply Mask	$x \cdot \sigma(\text{MLP}(x))$	$[B, T{\cdot}N, C]$
Mamba Encoder (depth = l_e)	$\text{Block}_1 \to \cdots \to \text{Block}_{l_e}$	$[B, T{\cdot}N, C]$
Mamba Decoder (depth = l_d)	$\text{Block}_1 \to \cdots \to \text{Block}_{l_d}$	–
- Decoder Queries	$Q =$ Embedding(N_q)	$[N_q, B, C]$
- Decoder EQ-Mamba	Q'	$[N_q, B, C]$
- Decoder QVI-Mamba	Concat(Q', M)	$[N_q + M, B, C] \to [N_q, B, C]$
- Decoder FFN	F	$[N_q, B, C]$
Prediction Heads	Class: Linear(F)	$[B, N_q, \text{num\_classes} + 1]$
	Box: MLP(F)	$[B, N_q, 4]$ (normalized)

Decoder. Our decoder, as depicted in Figure 2, uses the Mamba operator to process queries and integrate video information. Given an input sequence $x \in \mathbb{R}^{L \times d}$, the Mamba block computes its output $y \in \mathbb{R}^{L \times d}$ via a state-space model:

$$\begin{aligned} h_t &= \mathbf{A} \cdot h_{t-1} + \mathbf{B} \cdot x_t \\ y_t &= \mathbf{C} \cdot h_t \end{aligned} \tag{1}$$

where $\mathbf{A}, \mathbf{B}, \mathbf{C} \in \mathbb{R}^{d \times d}$ are learnable transition and projection matrices, and h_t is the hidden state at time step t. Compared with attention-based modules, this formulation enables linear-time complexity in sequence length L.

In the decoder design, Mamba serves two key functions: (1) linear transformation, and (2) feature extraction and sequence modeling based on selective copying [6]. EQ-Mamba primarily uses the first function, while QVI-Mamba exploits the second. Additionally, the concatenation of query and video information in the decoder draws inspiration from [7]. The decoder, consisting of l_d layers, is evaluated through ablation studies in Section 3.4 and A.4. Specifically, EQ-Mamba operates solely

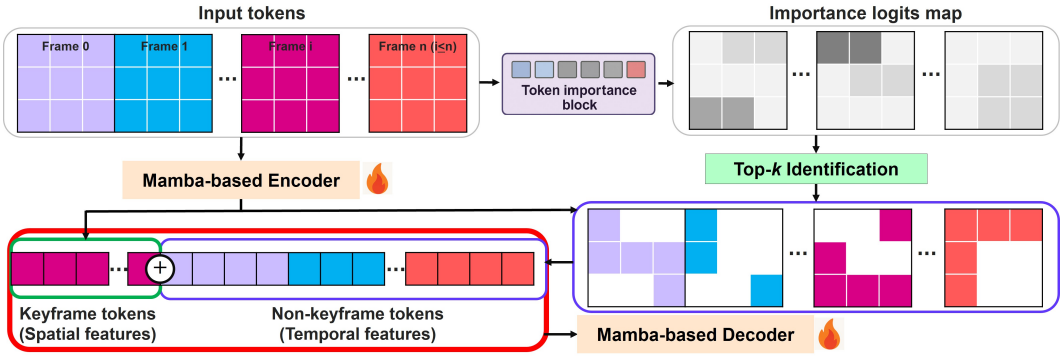

Figure 3: **Structure of the video token construction mechanism.** This module enables the decoder to obtain sufficient and effective information for action detection. Sufficient information is ensured by incorporating the complete spatial features of the keyframe (prediction frame), while redundancy reduction is achieved by filtering encoder tokens through token importance block. Importance scores are computed for each token in the encoder, retaining only the top-k highest-scoring tokens to supply temporal information. These tokens are then combined with a fixed keyframe memory portion, which preserves semantic context.

on the query embeddings, projecting and refining them within their own latent space. This process resembles self-attention in its focus on intra-query relationships but relies on Mamba's state-space modeling instead of attention mechanisms, enabling efficient linear transformations of the query tokens. QVI-Mamba integrates the refined query embeddings with the encoder's video features (hidden states), concatenating them to create a mixed representation that captures both query-specific information and video context. Finally, the FFN processes the output of the QVI-Mamba block, further transforming the fused representations to predict bounding boxes and class probabilities.

The key difference between Mamba and Transformer architectures underpins our design choices. While Transformers serve as attention and correlation mechanisms between tokens, Mamba relies on its unique mechanism of information storage and linear transformation via state-space dynamics.

2.3 Video Token Construction Mechanism

Prior work [4] shows that employing a token-importance mechanism improves performance over processing all tokens. In this work, to optimize token utilization, we introduce a token importance module. This module selects the most relevant tokens from the encoder, which aggregates tokens from different spatiotemporal frames, to enhance the decoder's ability to capture salient features. In encoder, it employs an MLP to compute importance logits for each token, followed by a sigmoid activation to derive importance scores. It should be noted that this part consists of learnable parameters, which are dynamically adjusted based on the token importance loss. For details on the computation of the loss, refer to Section 2.4. The decoder's input tokens are derived by selecting high-scoring tokens based on their importance, resulting in a more informative and compact representation for processing, as shown in Figure 3.

Specifically, we compute importance scores for each token in the encoder, and then guide the token selection process in the decoder. To preserve the features learned from the large-scale pretraining model, we do not reduce the number of tokens in the encoder; instead, token importance serves only as an indicator at this stage. The importance scores are directed by a learnable mechanism. After calculating the importance scores, we perform token selection by picking the top k percentage of tokens with the highest importance scores for each frame, keeping only the most informative tokens for further processing in the decoder. To further enhance this process, we combine a fixed portion of the memory, which contains all the keyframe tokens, with the selected tokens. The keyframes are crucial as they contain the accurate semantic information for the current frame. Next, we describe this process in tensor notation. For a batch of size B, the encoder processes a total of $T \times N_f$ tokens, where T is the frame number, and N_f is the number of tokens per frame. The token importance block assigns an importance score to each token (derived via the learnable MLP with sigmoid activation). Based on a top-k selection strategy (k is evaluated through ablation studies in Section 3.4.), we retain $\lfloor k \cdot N_f \rfloor$ tokens per frame. These selected tokens, totaling $N_s = \lfloor k \cdot (T \cdot N_f) \rfloor$, are concatenated with the keyframe tokens (fixed at N_f per keyframe).

2.4 Loss Functions

Since Mamba does not possess an intrinsic attention-based importance mechanism as Transformers do, this section seeks to answer the question: what constitutes important or relevant tokens? We do so under the premise that the L2 magnitude of a token does not directly represent its actual importance. Our training objective comprises two parts:

Detection Loss ($\mathcal{L}_1$): We adopt a DETR-style loss to supervise the action detection, which integrates three components: classification, bounding box position, and overlap, assigned weights of w_{cls}, w_{box}, and w_{ovl}, respectively. A Hungarian Matcher is employed to align predictions with ground-truth targets. These weight values are ablated in our ablation experiments to optimize performance, as we do not directly adopt coefficients from prior DETR-based works (e.g., [2], [12]), given that our loss function is newly designed to suit the Mamba-based architecture. There's also a weight for the *no-object* class.

Token Importance Loss ($\mathcal{L}_{\text{importance}}$): To learn token importance scores, we construct a binary ground-truth mask $y_i^{(b)}$ for each token i in sample b, indicating whether the token's center coordinates fall inside any ground-truth bounding box. Let $\alpha_i^{(b)}$ be the raw logit from the MLP for token i in sample b. We compute the binary cross-entropy loss:

$$\mathcal{L}_{\text{importance}} = -\frac{1}{BN}\sum_{b=1}^{B}\sum_{i=1}^{N}\Big[y_i^{(b)}\log(\sigma(\alpha_i^{(b)})) + \big(1-y_i^{(b)}\big)\log\big(1-\sigma(\alpha_i^{(b)})\big)\Big] \tag{2}$$

where B is the batch size, N is the total number of tokens per sample, and $\sigma(\cdot)$ is the logistic sigmoid.

Total Loss: The final loss combines the two objectives:

$$\mathcal{L} = \mathcal{L}_1 + \lambda \cdot \mathcal{L}_{\text{importance}}, \tag{3}$$

where λ balances action detection performance and token importance learning, which is evaluated through ablation studies in Section 3.4.

Mamba lacks an attention map, unlike Transformers, which use attention scores to represent token importance. Transformers motivated us to design token importance. The proposed token importance block is not an off-the-shelf, plug-and-play module, but a learning-based, multi-stage system requiring end-to-end training. The key steps are:

(1) Encoder-side importance calculation. The encoder includes a trainable MLP that outputs a continuous importance value for each token, supervised by our custom loss.

(2) Token selection in the decoder. The learned importance scores are used to select important tokens from the non-keyframes, which are concatenated with the keyframe tokens as the decoder input.

(3) Loss design. The overall loss combines standard action detection loss and token importance loss. The optimal loss ratio is determined through ablation studies.

This system's effectiveness relies on the synergy of all its components and joint training.

3 Experiments

3.1 Experimental Setup

We evaluate our MOGO on three common datasets for video action detection: JHMDB [10], UCF101-24 [11] and AVA [13]. JHMDB contains 928 trimmed videos from 21 action classes. We follow the data annotation and procedure outlined in [14]. UCF101-24 comprises 3,207 videos spanning 24 sports classes. Following standard practice, we report performance on split-1. AVA is a large-scale benchmark and contains 299 15-minute videos, divided into 211k training clips and 57k validation clips. The results for AVA are shown in Section 4. We evaluate performance with mAP under an IoU threshold of 0.5 on NVIDIA A40 GPUs. Other implementation details are shown in Section A.3.

Table 2: **Efficiency analysis of MOGO.**

Module	#Param	GFLOPs
Encoder	73.996M	101
Query_embed	57.6K	-
Decoder	7.228M	2.297
Class_embed	13.271K	1.325e-3
Bbox_embed	0.667M	6.659e-2
Overall	81.962M	104

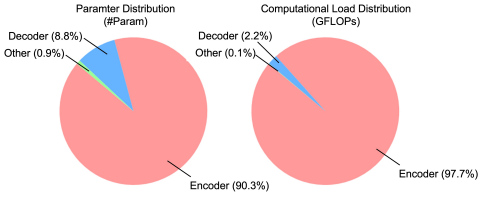

Figure 4: **Breakdown of parameter and computational distribution across components.** Based on the pretrained encoder, only a small amount of extra computation is added while still achieving good performance.

3.2 Efficiency Analysis

To assess the computational efficiency of MOGO, we measure the number of parameters, GFLOPs and inference speed and follow the code procedure in [7].

First, Table 2 details the parameters and GFLOPs for the model and its key modules. The entire MOGO model comprises 81.962 million parameters and incurs around 104 GFLOPs, reflecting a lightweight design compared to SOTA methods (see Section 3.3). The encoder dominates the computational load, accounting for roughly 97.7% of the total FLOPs as shown in Figure 4, as the encoder processes the 8-frame input using the pretrained Mamba-based backbone. In contrast, the decoder is significantly lighter, with 7.228M parameters and 2.297 GFLOPs, while auxiliary components like query_embed (57.6K parameters), class_embed (13.271K parameters), and bbox_embed (0.667M parameters) contribute minimally to the overall computational cost. This means that, based on the pretrained encoder, we only added a small amount of extra computation but still achieving good precision performance.

Second, we benchmark the inference speed using the throughput protocol defined in [4] with a video clip length of 8 frames. We run the model with 3 warm-up iterations and compute the average inference time over 10 additional runs. Our results show that MOGO achieves an average latency of 3.9 ms/img, corresponding to a throughput of 256 img/s. As shown in Table 3, this performance surpasses existing transformer-based methods: EVAD [4] (240 img/s on ViT-B), WOO [5] (176 img/s on ViT-B, 147 on SF-R101), and TubeR [3] (64 img/s). While EVAD reports a peak throughput of 334 img/s under certain alternative configurations, our approach remains highly competitive, even though the current version of Mamba's CUDA/C++ kernels still has limitations in parallel processing relative to Transformer implementations.

3.3 Comparison with SOTA Methods

Table 3: **Comparison of MOGO with SOTA methods.** GFLOPs are reported where available. Art.: Architecture, Thrp.: Throughput. C: CNN, T: Transformer, M: Mamba. dec.: decoder. Cv.: The original work only reported GFLOPs based on image-based RGB input, which has been converted here. J: JHMDB, U: UCF101-24.

(a) Comparison on efficiency.

Model	Art.	Backbone	#Param	GFLOPs	Thrp.
SlowFast [15]	C	SF-R101-NL	-	234×30	-
MOC [14]	C	DLA34	-	235.2 [Cv.]	-
MaskFeat [16]	T	MViTv2-L	218M	2828	-
EVAD [4]	T	ViT-L	185M (dec.)	737	153
MeMViT [17]	T	MViTv2	52.6M	620	-
VideoMAE [18]	T	ViT-L	305M	597	-
WOO [5]	T	ViT-B	314M (head)	378	176
WOO [5]	T	SF-R101	314M (head)	252	147
EVAD [4]	T	ViT-B	185M (dec.)	243	240
TubeR [3]	T	CSN-152	-	240	64*
Ours (MOGO)	M	Mamba-M	**82M**	**102–104**	**256**

(b) Comparison on performance.

Model	Art.	Backbone	Pre-train	f-mAP (J)	f-mAP (U)
EESSL [19]	C	I3D-CNN	-	64.4	69.9
ACT [20]	C	VGG	-	65.7	69.5
SMT [21]	C	I3D-CNN	K400	69.8	73.9
MOC [14]	C	DLA34	-	70.8	78.0
AVA [13]	C	I3D-VGG	-	73.3	76.3
STAD [22]	T	ViT-B	InternVid	61.4	71.6
WOO [5]	T	SF-R101	K600	80.5	76.7*
TubeR [3]	T	I3D	IG+K400	80.7	81.3
Ours (MOGO)	M	Mamba-B	K400	**76.7**	**78.2**

*: measured by [4].

We evaluate our MOGO model against SOTA methods on two datasets, with results summarized in Table 3. Our approach achieves an mAP of 76.7 on JHMDB while maintaining a low computational cost of 102-104 GFLOPs, leveraging an 8-frame Mamba-based backbone. Although our mAP is

slightly lower than top-performing Transformer-based methods such as WOO (80.5) and TubeR (80.7), these models rely on heavier architectures (e.g., ViT-B), which may increase computational overhead. In contrast, our model surpasses all CNN-based methods on JHMDB dataset, including I3D-CNN architectures like EESSK (64.4), and ACT (65.7), demonstrating the superior efficiency of Mamba-based modeling over conventional convolution designs. Compared to WOO (SFR101) and TubeR (CSN-152), our MOGO model reduces GFLOPs by approximately 60% and 57%, respectively, while only sacrificing 3.8–4.0 mAP points (from 80.5 to 76.7 for WOO, and 80.7 to 76.7 for TubeR) on the JHMDB dataset. Compared to TubeR (I3D), our MOGO model only sacrifices 3.1 mAP points on the UCF101-24 dataset. Part of this gap likely reflects the availability of strong Transformer pretraining (e.g., IG+K400) leveraged by TubeR and other Transformer-based methods, whereas comparable large-scale pretrained checkpoints for Mamba are still scarce.

Comparison on GPU Memory Usage with EVAD [4]. We evaluate GPU memory consumption using the same settings as EVAD (an efficient video action detection method with significant performance improvements using Transformer), employing a single GPU with a batch size of 8. Both methods adopt token reduction strategy, where tokens are removed according to predefined rules. The results in Figure 5 demonstrate that: first, our method consistently consumes less GPU memory compared to EVAD. EVAD requires around 1.6 times more memory than our method, when token retention ratio is 0.4. Second, as the number of retained tokens increases, the GPU memory usage of EVAD grows significantly. In the extreme case where all tokens are retained, EVAD requires 2.8 times more memory than our method. Therefore, MOGO maintains lower and stable GPU memory footprints compared to EVAD. **That means under the same hardware and experimental conditions, it can employ larger batch sizes to improve performance further.**

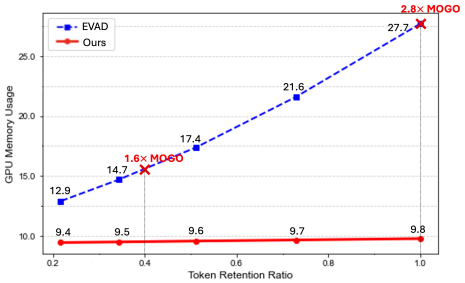

Figure 5: **Comparison of GPU memory usage between our method and EVAD under different token retention ratios.**

3.4 Ablation Studies

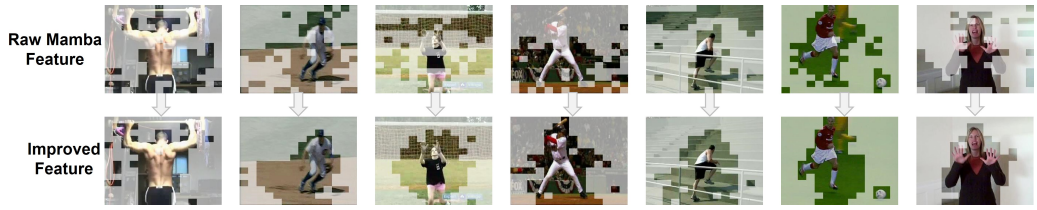

Figure 6: **Qualitative ablation: visualization of the impact of the token importance mechanism.** Row 1 shows raw Mamba outputs without the loss guidance. Row 2 shows outputs with our proposed importance modeling. Tokens inside target regions are more emphasized.

Qualitative Ablation. Unlike Transformers, which rely on attention mechanisms to compute token-to-token interactions, Mamba encodes temporal dependencies implicitly through sequential modeling. This makes it challenging to directly interpret token importance. As shown in the first row of Figure 6, raw Mamba outputs tend to produce scattered and less structured token representations. To address this, we propose a heuristic loss function (see Sec. 2.4), which encourages tokens inside the ground truth bounding boxes to receive higher importance. Furthermore, to avoid introducing significant computational overhead, we insert a lightweight MLP directly before the encoder tokens as shown in Table 1. This MLP outputs a token-wise importance score, which is then multiplied element-wise with the encoder tokens. With this, as shown in the second row of Figure 6, the token activations become more focused on semantically meaningful regions. More examples are provided in Figure S4.

Quantitative Ablation. The following ablation experiments are conducted on the JHMDB dataset. The findings are summarized in Table 4.

Pretrained models. Table 4(a) presents the results of ablation experiments conducted on pretrained models. All models employ a Mamba-based middle-sized model as the backbone, pretrained on

Table 4: **Quantitative ablation: experiments results.** (a) Pretrained models. Using different pretrained models as the encoder. MFT: mask with fine-tuning, MPT: mask with pretraining. (b) Encoder depth. enc.: encoder. (c) Decoder components. The EQ-Mamba and QVI-Mamba components are critical design elements. These components are evaluated by removing each one individually to assess their impact on the model's performance. dec.: decoder, md.: model, rmd.: removed. (d) Decoder input: temporal info. In the decoder, the top $k\%$ of tokens are selected and integrated with keyframe tokens. (e) Decoder input: keyframe info. Ex.: Exchange token positions of keyframe and temporal info. (f) Query number. (g) Ratio of total loss.

(a) Pretrained models.

Model	Baseline	MFT	MPT
mAP	51.7	65.0	31.2

(b) Encoder depth.

l_e	mAP	enc.GFLOPs (#param)
24	60.4	76 (55.721M)
32	66.2	101 (73.996M)
40	61.1	126 (92.271M)

(c) Decoder components.

Case	dec.GFLOPs	md.GFLOPs
EQ rmd.	2.098	103
QVI rmd.	0.466	102
Proposed	2.297	104

(d) Decoder input: temporal info.

k	mAP	dec.GFLOPs(#Param)	md.GFLOPs
5	66.4	1.198 (7.228M)	103
10	66.8	1.357 (7.228M)	103
20	67.1	1.676 (7.228M)	103
40	67.4	2.297 (7.228M)	104
50	66.5	2.616 (7.228M)	104
70	65.6	3.237 (7.228M)	105

(e) Decoder input: keyframe info.

Case	Removed	Ex.	Proposed
mAP	53.7	53.9	69.0

(f) Query number.

Case	50	100	200
mAP	58.5	66.0	61.3

(g) Ratio of total loss.

λ	0.1	0.5	1	2
mAP	73.3	75.6	74.4	74.4

the K400 dataset [23] with a resolution of 224×224. The baseline model achieves a mAP of 51.7. Introducing a mask with fine-tuning significantly boosts the mAP to 65.0. In contrast, using a mask with pretraining yields a decrease, achieving an mAP of 31.2. These results suggest that fine-tuning with masking is more effective than pretraining, likely due to better adaptation to the target task. Further discussion about pretrained models can be found in Section 4.

Encoder depth. The results in Table 4(b) indicate that using 32 layers in the encoder achieves the highest mAP of 66.2, with an encoder computational cost of 101 GFLOPs (73.996M parameters) and a model-level cost of 104 GFLOPs. Increasing the depth to 40 layers results in performance degradation (mAP 61.1) despite a higher computational cost of 126 GFLOPs (92.271M parameters), likely due to overfitting. Therefore, we set the encoder depth to 32 as the default.

Decoder components. Table 4 (c) investigates the decoder structure by ablating key components, EQ-Mamba (EQ) and QVI-Mamba (QVI), and comparing them against the proposed design. Removing EQ-Mamba or QVI-Mamba reduces the mAP significantly (possible theoretical reason is that removing EQ is equivalent to a random query directly entering Mamba, while removing QVI is equivalent to using inadequate video information), although decoder GFLOPs drops slightly. This demonstrates that every component of our design is indispensable but lightweight, further validating the correctness of our extrapolation from Transformer to Mamba as depicted in Figure 1.

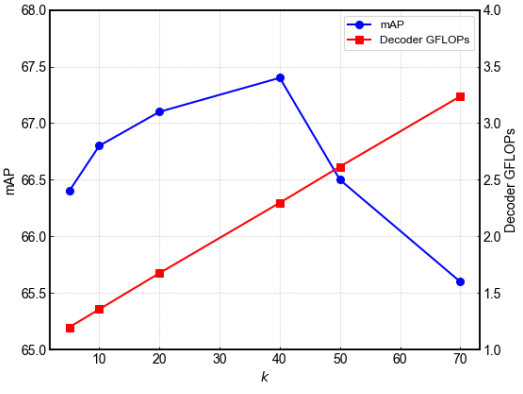

Figure 7: **The trends of mAP and decoder GFLOPs with varying numbers of retained non-keyframe tokens.** It demonstrates the importance of video feature tokens from non-keyframes as temporal information. We evaluate the impact of selecting the top $k\%$ of tokens.

Decoder input: temporal information. Table 4 (d) evaluates the impact of selecting the top $k\%$ of non-keyframe tokens in the decoder, which are integrated with keyframe tokens for processing. As k increases from 5 to 70, the mAP improves from 66.4 to a peak of 67.4 at k=40, while decoder GFLOPs rise from 1.198 to 3.237, with the number of parameters remaining constant at 7.228M and model GFLOPs slightly increasing from 103 to 105. Beyond k=40, the mAP declines to 66.5 at k=50 and further to 65.6 at k=70, despite higher computational costs. This indicates that k=40 strikes an optimal balance between performance and efficiency, making it the most effective choice for this strategy. Figure 7 demonstrates the importance

of video information from frames other than the keyframe as temporal information. Intuitively, this drop when k>40 occurs because k controls only the retention of non-keyframe tokens. We keep all keyframe tokens and perform detection on the keyframe, while non-keyframes serve primarily as contextual support. As k increases, more low-utility background tokens from non-keyframes are admitted, which can dilute salient cues and slightly reduce performance.

Decoder input: keyframe information. Table 4 (e) compares different configurations of keyframe information usage. The one with keyframe information removed achieves an mAP of 53.7, while exchanging the token positions of the keyframe information and the temporal information (Ex.) slightly improves the mAP to 53.9. In contrast, the initial arrangement outperforms both alternatives with an mAP of 69.0. This performance gap demonstrates that the proposed design, leveraging the full potential of keyframe information, is the most effective approach for video token construction.

Query number. Table 4 (f) evaluates the effect of varying the number of queries on model performance. This limitation of using a fixed number of queries is discussed in Section 5.

Ratio of total loss. Due to our redesign of the loss function, the relationships between the different components have also changed, making the final results sensitive to the choice of weights. Therefore, a re-evaluation of the weight configurations is necessary to optimize performance. The findings are summarized in Table 4 (g), with parameters defined in Section 2.4. For the total loss ratio, adjusting λ reveals that 0.5 is the optimal choice, achieving the highest mAP of 75.6.

4 Discussion

First, we discuss *innovation 1: pure Mamba-based architecture*:

Extension to multi-label detection. MOGO is originally designed for end-to-end detection, while AVA involves multi-label prediction per bounding box. To further evaluate adaptability, we modified the existing decoder to support multiple labels per bounding box without introducing an explicit classification branch. Corresponding adjustments were made to the loss and training setup. On the AVAv2.2 validation set, the adapted MOGO achieved an mAP of 16.2 (at step 26). This shows that MOGO can extend to multi-label settings with competitive accuracy. Training logs are presented in Figure S6. Another Mamba-based work [24] has reported their evaluations; however, a fair comparison would require additional details (e.g., architectural specifications and FLOPs calculation).

Comparison with FlashAttention. This comparison assesses how an optimized Transformer baseline performs relative to Mamba. We implemented a decoder variant that replaces the Mamba blocks with FlashAttention 2.8.2 (non-causal). The modified decoder reduces parameters from 7.228M to 5.321M and GFLOPs from 2.297 to 1.116, indicating higher computational efficiency. Trained on JHMDB with 4 × A40 GPUs for 50 epochs and a batch size of 32, it achieves an mAP of 70.1 (Initial loss: 7.7654, grad norm: 14.1749 → Final loss: 0.4765, grad norm: 1.8073). While FlashAttention offers higher efficiency, its mAP does not surpass our Mamba-based decoder. However, this motivates improving Mamba's low-level C++/CUDA kernels.

Table 5: **Performance on longer video sequences.**

Ex.	Frames	Pretrained Model	Batch Size	mAP
1	16	K400	16	69.50
2	64	Breakfast-actions-dataset	4	41.90
3	64	K400	4	63.43

Performance on longer video sequences and varying pretraining models. We conducted experiments on longer video sequences using the UCF101-24 dataset. For each setup, we employed a corresponding pre-trained encoder from [7] and adjusted the decoder accordingly. All experiments were trained for 30 epochs on 2 NVIDIA A40 GPUs. The configurations and results are summarized in Table 5. These results indicate that our method maintains good performance on longer video sequences. Moreover, we observed that the choice of pre-trained model plays a crucial role: using K400 pretraining yields higher accuracy than using the Breakfast dataset [25]. To further investigate this factor, we trained with a new encoder pretrained on the SSV2 dataset [26] (2 A40 GPUs, 50 epochs, batch size 30) and obtained an f-mAP of only 64.1 on JHMDB (Initial loss: 7.9834, grad norm: 67.6360 → Final loss: 0.4847, grad norm: 6.6854). The results confirm that K400 pretraining remains superior to SSV2 in our setting.

Training with long frames and autoregressive tracking. Autoregressive trackers such as TrackFormer [27] propagate track queries frame-by-frame to jointly detect and track objects across long videos without fixing a global clip length, illustrating an alternative way to scale beyond 64 frames. In contrast, our method currently relies on publicly available pretrained encoders [7], whose checkpoints

are trained for inputs up to 64 frames. Since action-detection mAP is highly sensitive to the encoder's pretraining quality and capacity, this limitation arises from data and model availability rather than the framework itself. In principle, our pipeline can process much longer sequences.

Bidirectional scan in the encoder. Our encoder employs a bidirectional scan. In Mamba, this means that at each position a forward state summarizes all preceding tokens and a backward state summarizes all following tokens; the token representation is then obtained by fusing these two states. As a result, each token can store richer information.

Next, we discuss *Innovation 2: video token construction mechanism*:

Rethinking token selection: RLT-based and random token selection. Inspired by Run-Length Tokenization (RLT) [28], we replace our original decoder-side token selection with two key components: (i) *token selection*, which prunes temporally redundant tokens while retaining tokens that change semantically across frames; and (ii) *run-length embedding*, which encodes how long a selected token remains stable and injects this temporal continuity into the token features before decoding. On JHMDB (4 GPUs, 60 epochs, batch size 32), this variant reaches an f-mAP of 72.1 (Initial loss: 8.4603, grad norm: 143.7739 $\rightarrow$ Final loss: 0.4385, grad norm: 2.4390). While slightly below our best MOGO configuration, these results indicate that combining RLT-style token selection with run-length information is a promising direction for further improvement. The above is a heuristic attempt. For a stochastic baseline, we removed importance logits and randomly retained a fixed proportion of tokens per frame (40%), keeping all other settings identical to Figure 7. Trained for 30 epochs, this random-selection variant achieved an f-mAP of 67.2 (Initial loss: 7.9832 $\rightarrow$ Final loss: 0.6982). Under the same environment and retention ratio, our importance-guided selection attains 67.4 mAP, indicating a consistent gain over random sampling.

Generalizing the token-importance block to other methods. To broaden applicability beyond our own architecture, we integrate the token-importance module into TubeR [3] and evaluate on JHMDB, comparing the standard full-token setting with variants that retain only a subset of non-keyframe tokens. Using the released JHMDB-pretrained CSN-152 checkpoint, the detector attains 71.2 mAP after one epoch. We therefore adopt the pretrained setting as the full-token baseline. With our importance scores guiding token reduction, keeping 80% of non-keyframe tokens yields 72.05 mAP, and keeping 40% yields 72.0 mAP. Note that while the Transformer in TubeR inherently possesses an attention-based token importance mechanism, we align its setup with our proposed method by using the outputs of the trainable MLP to represent token importance within the encoder. The intermediate frames are also designated as key frames. For the loss, however, we adhere to the original TubeR implementation. These results are on par with the full-token baseline in small-scale experiments.

Keyframe-centric detection without an action-switch head. Our approach does not employ an explicit *action-switch head*; instead, it follows a DETR-style formulation with Hungarian matching over class logits and bounding box predictions. Conceptually, the method can be viewed as image-style action detection: we predict on a designated keyframe (typically the middle frame) while importing **contextual tokens** from preceding and following frames. This design helps the model sense how a person's action shifts across time, but it does not explicitly model precise action boundaries or subtle temporal transitions.

5 Conclusion and Future Work

Our proposed MOGO framework introduces a pure Mamba-based architecture for end-to-end video action detection, eliminating reliance on Transformer components. This design addresses limitations noted in prior work, such as the complexity overhead in [4], by leveraging Mamba's state-space modeling for efficient processing of video sequences. This results in a significant reduction in computation while maintaining competitive precision. Additionally, our video token construction mechanism can obtain important token information across spatiotemporal frames. In this way, important cues (closely related to the action prediction) can be effectively retained.

MOGO's performance is among the top-tier Transformer-based methods, though it has not surpassed the very best ones. This limitation stems from two factors: first, GFLOPs reduction may trade off some precision; second, the scarcity of pre-trained Mamba models limits feature representation quality, unlike the extensive pretraining pools available for Transformers. A further limitation is the use of a fixed query; in its current form, the model cannot reliably handle scenes with more than 100 people. However, this study highlights Mamba's promise in this new field. Future work will focus on developing richer pretrained models to help enhance performance.

Acknowledgments and Disclosure of Funding

Funding: This work received no third-party funding or support. **Competing Interests:** The authors declare no competing interests.

References

[1] Zhen Hao Sia and Yogesh Singh Rawat. Scaling open-vocabulary action detection. *arXiv preprint arXiv:2504.03096*, 2025.

[2] Nicolas Carion, Francisco Massa, Gabriel Synnaeve, Nicolas Usunier, Alexander Kirillov, and Sergey Zagoruyko. End-to-end object detection with transformers. In *Proceedings of the European Conference on Computer Vision (ECCV)*, 2020.

[3] Jiaojiao Zhao, Yanyi Zhang, Xinyu Li, Hao Chen, Bing Shuai, Mingze Xu, Chunhui Liu, Kaustav Kundu, Yuanjun Xiong, Davide Modolo, Ivan Marsic, Cees G. M. Snoek, and Joseph Tighe. TubeR: Tubelet transformer for video action detection. In *Proceedings of the IEEE/CVF Conference on Computer Vision and Pattern Recognition (CVPR)*, 2022.

[4] Lei Chen, Zhan Tong, Yibing Song, Gangshan Wu, and Limin Wang. Efficient video action detection with token dropout and context refinement. In *Proceedings of the IEEE/CVF International Conference on Computer Vision (ICCV)*, 2023.

[5] Shoufa Chen, Peize Sun, Enze Xie, Chongjian Ge, Jiannan Wu, Lan Ma, Jiajun Shen, and Ping Luo. Watch only once: An end-to-end video action detection framework. In *Proceedings of the IEEE/CVF International Conference on Computer Vision (ICCV)*, 2021.

[6] Albert Gu and Tri Dao. Mamba: Linear-time sequence modeling with selective state spaces. *arXiv preprint arXiv:2312.00752*, 2023.

[7] Kunchang Li, Xinhao Li, Yi Wang, Yinan He, Yali Wang, Limin Wang, and Yu Qiao. Videomamba: State space model for efficient video understanding. *arXiv preprint arXiv:2403.06977*, 2024.

[8] Arkaprava Sinha, Monish Soundar Raj, Pu Wang, Ahmed Helmy, and Srijan Das. MS-Temba: Multi-scale temporal mamba for efficient temporal action detection. *arXiv preprint arXiv:2501.06138*, 2025.

[9] Alexey Dosovitskiy, Lucas Beyer, Alexander Kolesnikov, Dirk Weissenborn, Xiaohua Zhai, Thomas Unterthiner, Mostafa Dehghani, Matthias Minderer, Georg Heigold, Sylvain Gelly, Jakob Uszkoreit, and Neil Houlsby. An image is worth 16x16 words: Transformers for image recognition at scale. In *International Conference on Learning Representations (ICLR)*, 2021.

[10] Hueihan Jhuang, Juergen Gall, Silvia Zuffi, Cordelia Schmid, and Michael J. Black. Towards understanding action recognition. In *Proceedings of the IEEE International Conference on Computer Vision (ICCV)*, 2013.

[11] Khurram Soomro, Amir Roshan Zamir, and Mubarak Shah. Ucf101: A dataset of 101 human actions classes from videos in the wild. *arXiv preprint arXiv:1212.0402*, 2012.

[12] Depu Meng, Xiaokang Chen, Zejia Fan, Gang Zeng, Houqiang Li, Yuhui Yuan, Lei Sun, and Jingdong Wang. Conditional DETR for fast training convergence. In *Proceedings of the IEEE/CVF International Conference on Computer Vision (ICCV)*, 2021.

[13] Chunhui Gu, Chen Sun, David A. Ross, Carl Vondrick, Caroline Pantofaru, Yeqing Li, Sudheendra Vijayanarasimhan, George Toderici, Susanna Ricco, Rahul Sukthankar, Cordelia Schmid, and Jitendra Malik. AVA: A video dataset of spatio-temporally localized atomic visual actions. In *Proceedings of the IEEE Conference on Computer Vision and Pattern Recognition (CVPR)*, 2018.

[14] Yixuan Li, Zixu Wang, Limin Wang, and Gangshan Wu. Actions as moving points. In *Proceedings of the European Conference on Computer Vision (ECCV)*, 2020.

[15] Christoph Feichtenhofer, Haoqi Fan, Jitendra Malik, and Kaiming He. SlowFast networks for video recognition. In *Proceedings of the IEEE/CVF International Conference on Computer Vision (ICCV)*, 2019.

[16] Chen Wei, Haoqi Fan, Saining Xie, Chao-Yuan Wu, Alan Yuille, and Christoph Feichtenhofer. Masked feature prediction for self-supervised visual pre-training. In *Proceedings of the IEEE/CVF Conference on Computer Vision and Pattern Recognition (CVPR)*, 2022.

[17] Chao-Yuan Wu, Yanghao Li, Karttikeya Mangalam, Haoqi Fan, Bo Xiong, Jitendra Malik, and Christoph Feichtenhofer. MeMViT: Memory-augmented multiscale vision transformer for efficient long-term video recognition. In *Proceedings of the IEEE/CVF Conference on Computer Vision and Pattern Recognition (CVPR)*, 2022.

[18] Zhan Tong, Yibing Song, Jue Wang, and Limin Wang. VideoMAE: Masked autoencoders are data-efficient learners for self-supervised video pre-training. In *Advances in Neural Information Processing Systems (NeurIPS 2022)*, 2022.

[19] Akash Kumar and Yogesh Singh Rawat. End-to-end semi-supervised learning for video action detection. In *Proceedings of the IEEE/CVF Conference on Computer Vision and Pattern Recognition (CVPR)*, 2022.

[20] Vicky Kalogeiton, Philippe Weinzaepfel, Vittorio Ferrari, and Cordelia Schmid. Action tubelet detector for spatio-temporal action localization. In *Proceedings of the IEEE International Conference on Computer Vision (ICCV)*, 2017.

[21] Akash Kumar, Sirshapan Mitra, and Yogesh Singh Rawat. Stable mean teacher for semi-supervised video action detection. *arXiv preprint arXiv:2412.07072*, 2024.

[22] Tao Wu, Shuqiu Ge, Jie Qin, Gangshan Wu, and Limin Wang. Open-vocabulary spatio-temporal action detection. *arXiv preprint arXiv:2405.10832*, 2024.

[23] Will Kay, João Carreira, Karen Simonyan, Brian Zhang, Chloe Hillier, Sudheendra Vijayanarasimhan, Fabio Viola, Tim Green, Trevor Back, Paul Natsev, Mustafa Suleyman, and Andrew Zisserman. The kinetics human action video dataset. *arXiv preprint arXiv:1705.06950*, 2017.

[24] Jinyoung Park, Hee-Seon Kim, Kangwook Ko, Minbeom Kim, and Changick Kim. Videomamba: Spatio-temporal selective state space model. In *Proceedings of the European Conference on Computer Vision (ECCV)*, 2024.

[25] Hilde Kuehne, Ali Arslan, and Thomas Serre. The language of actions: Recovering the syntax and semantics of goal-directed human activities. In *Proceedings of the IEEE Conference on Computer Vision and Pattern Recognition (CVPR)*, 2014.

[26] Raghav Goyal, Samira Ebrahimi Kahou, Vincent Michalski, Joanna Materzynska, Susanne Westphal, Heuna Kim, Valentin Haenel, Ingo Fruend, Peter Yianilos, Moritz Mueller-Freitag, Florian Hoppe, Christian Thurau, Ingo Bax, and Roland Memisevic. The "something something" video database for learning and evaluating visual common sense. In *Proceedings of the IEEE International Conference on Computer Vision (ICCV)*, 2017.

[27] Tim Meinhardt, Alexander Kirillov, Laura Leal-Taixé, and Christoph Feichtenhofer. Trackformer: Multi-object tracking with transformers. In *Proceedings of the IEEE/CVF Conference on Computer Vision and Pattern Recognition (CVPR)*, 2022.

[28] Rohan Choudhury, Guanglei Zhu, Sihan Liu, Koichiro Niinuma, Kris M. Kitani, and László A. Jeni. Don't look twice: Faster video transformers with run-length tokenization. In *Proceedings of the 38th Conference on Neural Information Processing Systems (NeurIPS 2024)*, 2024.

[29] Lei Chen, Zhan Tong, Yibing Song, Gangshan Wu, and Limin Wang. CycleACR: Cycle modeling of actor-context relations for video action detection. *arXiv preprint arXiv:2303.16118*, 2023.

[30] Rohit Girdhar, João Carreira, Carl Doersch, and Andrew Zisserman. Video action transformer network. In *Proceedings of the IEEE/CVF Conference on Computer Vision and Pattern Recognition (CVPR)*, 2019.

[31] Hui Lu, Albert Ali Salah, and Ronald Poppe. Snakes and ladders: Two steps up for videomamba. *arXiv preprint arXiv:2406.19006*, 2024.

[32] Ali Hatamizadeh and Jan Kautz. MambaVision: A hybrid mamba-transformer vision backbone. *arXiv preprint arXiv:2407.08083*, 2024.

[33] Soumyabrata Chaudhuri and Saumik Bhattacharya. Simba: Mamba augmented u-shiftgcn for skeletal action recognition in videos. *arXiv preprint arXiv:2404.07645*, 2024.

[34] Xiuwei Chen, Wentao Hu, Xiao Dong, Sihao Lin, Zisheng Chen, Meng Cao, Yina Zhuang, Jianhua Han, Hang Xu, and Xiaodan Liang. Transmamba: Fast universal architecture adaption from transformers to mamba. *arXiv preprint arXiv:2502.15130*, 2025.

[35] Yuhui Lin, Jiaxuan Lu, Yue Yong, and Jiahao Zhang. Mv-gmn: State space model for multi-view action recognition. *arXiv preprint arXiv:2501.13829*, 2025.

NeurIPS Paper Checklist

1. **Claims**

   Question: Do the main claims made in the abstract and introduction accurately reflect the paper's contributions and scope?

   Answer: [Yes]

   Justification: They state the main contributions and scope of the paper.

   Guidelines:

   - The answer NA means that the abstract and introduction do not include the claims made in the paper.
   - The abstract and/or introduction should clearly state the claims made, including the contributions made in the paper and important assumptions and limitations. A No or NA answer to this question will not be perceived well by the reviewers.
   - The claims made should match theoretical and experimental results, and reflect how much the results can be expected to generalize to other settings.
   - It is fine to include aspirational goals as motivation as long as it is clear that these goals are not attained by the paper.

2. **Limitations**

   Question: Does the paper discuss the limitations of the work performed by the authors?

   Answer: [Yes]

   Justification: The paper discusses key limitations in Section 5.

   Guidelines:

   - The answer NA means that the paper has no limitation while the answer No means that the paper has limitations, but those are not discussed in the paper.
   - The authors are encouraged to create a separate "Limitations" section in their paper.
   - The paper should point out any strong assumptions and how robust the results are to violations of these assumptions (e.g., independence assumptions, noiseless settings, model well-specification, asymptotic approximations only holding locally). The authors should reflect on how these assumptions might be violated in practice and what the implications would be.
   - The authors should reflect on the scope of the claims made, e.g., if the approach was only tested on a few datasets or with a few runs. In general, empirical results often depend on implicit assumptions, which should be articulated.
   - The authors should reflect on the factors that influence the performance of the approach. For example, a facial recognition algorithm may perform poorly when image resolution is low or images are taken in low lighting. Or a speech-to-text system might not be used reliably to provide closed captions for online lectures because it fails to handle technical jargon.
   - The authors should discuss the computational efficiency of the proposed algorithms and how they scale with dataset size.
   - If applicable, the authors should discuss possible limitations of their approach to address problems of privacy and fairness.
   - While the authors might fear that complete honesty about limitations might be used by reviewers as grounds for rejection, a worse outcome might be that reviewers discover limitations that aren't acknowledged in the paper. The authors should use their best judgment and recognize that individual actions in favor of transparency play an important role in developing norms that preserve the integrity of the community. Reviewers will be specifically instructed to not penalize honesty concerning limitations.

3. **Theory assumptions and proofs**

   Question: For each theoretical result, does the paper provide the full set of assumptions and a complete (and correct) proof?

   Answer: [Yes]

Justification: This paper provides the full set of assumptions and a complete proof in Section 2.

Guidelines:

- The answer NA means that the paper does not include theoretical results.
- All the theorems, formulas, and proofs in the paper should be numbered and cross-referenced.
- All assumptions should be clearly stated or referenced in the statement of any theorems.
- The proofs can either appear in the main paper or the supplemental material, but if they appear in the supplemental material, the authors are encouraged to provide a short proof sketch to provide intuition.
- Inversely, any informal proof provided in the core of the paper should be complemented by formal proofs provided in appendix or supplemental material.
- Theorems and Lemmas that the proof relies upon should be properly referenced.

4. **Experimental result reproducibility**

   Question: Does the paper fully disclose all the information needed to reproduce the main experimental results of the paper to the extent that it affects the main claims and/or conclusions of the paper (regardless of whether the code and data are provided or not)?

   Answer: [Yes]

   Justification: We provide full implementation details in Section 2 and Section A.3.

   Guidelines:

   - The answer NA means that the paper does not include experiments.
   - If the paper includes experiments, a No answer to this question will not be perceived well by the reviewers: Making the paper reproducible is important, regardless of whether the code and data are provided or not.
   - If the contribution is a dataset and/or model, the authors should describe the steps taken to make their results reproducible or verifiable.
   - Depending on the contribution, reproducibility can be accomplished in various ways. For example, if the contribution is a novel architecture, describing the architecture fully might suffice, or if the contribution is a specific model and empirical evaluation, it may be necessary to either make it possible for others to replicate the model with the same dataset, or provide access to the model. In general. releasing code and data is often one good way to accomplish this, but reproducibility can also be provided via detailed instructions for how to replicate the results, access to a hosted model (e.g., in the case of a large language model), releasing of a model checkpoint, or other means that are appropriate to the research performed.
   - While NeurIPS does not require releasing code, the conference does require all submissions to provide some reasonable avenue for reproducibility, which may depend on the nature of the contribution. For example
     (a) If the contribution is primarily a new algorithm, the paper should make it clear how to reproduce that algorithm.
     (b) If the contribution is primarily a new model architecture, the paper should describe the architecture clearly and fully.
     (c) If the contribution is a new model (e.g., a large language model), then there should either be a way to access this model for reproducing the results or a way to reproduce the model (e.g., with an open-source dataset or instructions for how to construct the dataset).
     (d) We recognize that reproducibility may be tricky in some cases, in which case authors are welcome to describe the particular way they provide for reproducibility. In the case of closed-source models, it may be that access to the model is limited in some way (e.g., to registered users), but it should be possible for other researchers to have some path to reproducing or verifying the results.

5. **Open access to data and code**

   Question: Does the paper provide open access to the data and code, with sufficient instructions to faithfully reproduce the main experimental results, as described in supplemental material?

Answer: [Yes]

Justification: The paper provides open access to its code in the abstract.

Guidelines:

- The answer NA means that paper does not include experiments requiring code.
- Please see the NeurIPS code and data submission guidelines (`https://nips.cc/public/guides/CodeSubmissionPolicy`) for more details.
- While we encourage the release of code and data, we understand that this might not be possible, so "No" is an acceptable answer. Papers cannot be rejected simply for not including code, unless this is central to the contribution (e.g., for a new open-source benchmark).
- The instructions should contain the exact command and environment needed to run to reproduce the results. See the NeurIPS code and data submission guidelines (`https://nips.cc/public/guides/CodeSubmissionPolicy`) for more details.
- The authors should provide instructions on data access and preparation, including how to access the raw data, preprocessed data, intermediate data, and generated data, etc.
- The authors should provide scripts to reproduce all experimental results for the new proposed method and baselines. If only a subset of experiments are reproducible, they should state which ones are omitted from the script and why.
- At submission time, to preserve anonymity, the authors should release anonymized versions (if applicable).
- Providing as much information as possible in supplemental material (appended to the paper) is recommended, but including URLs to data and code is permitted.

6. **Experimental setting/details**

   Question: Does the paper specify all the training and test details (e.g., data splits, hyperparameters, how they were chosen, type of optimizer, etc.) necessary to understand the results?

   Answer: [Yes]

   Justification: All experimental settings are detailed in Section 3 and Section A.3.

   Guidelines:

   - The answer NA means that the paper does not include experiments.
   - The experimental setting should be presented in the core of the paper to a level of detail that is necessary to appreciate the results and make sense of them.
   - The full details can be provided either with the code, in appendix, or as supplemental material.

7. **Experiment statistical significance**

   Question: Does the paper report error bars suitably and correctly defined or other appropriate information about the statistical significance of the experiments?

   Answer: [Yes]

   Justification: For latency evaluation, we report the average inference time over multiple runs to account for runtime variability, as described in Section 3.2.

   Guidelines:

   - The answer NA means that the paper does not include experiments.
   - The authors should answer "Yes" if the results are accompanied by error bars, confidence intervals, or statistical significance tests, at least for the experiments that support the main claims of the paper.
   - The factors of variability that the error bars are capturing should be clearly stated (for example, train/test split, initialization, random drawing of some parameter, or overall run with given experimental conditions).
   - The method for calculating the error bars should be explained (closed form formula, call to a library function, bootstrap, etc.)
   - The assumptions made should be given (e.g., Normally distributed errors).

- It should be clear whether the error bar is the standard deviation or the standard error of the mean.
- It is OK to report 1-sigma error bars, but one should state it. The authors should preferably report a 2-sigma error bar than state that they have a 96% CI, if the hypothesis of Normality of errors is not verified.
- For asymmetric distributions, the authors should be careful not to show in tables or figures symmetric error bars that would yield results that are out of range (e.g. negative error rates).
- If error bars are reported in tables or plots, The authors should explain in the text how they were calculated and reference the corresponding figures or tables in the text.

8. **Experiments compute resources**

   Question: For each experiment, does the paper provide sufficient information on the computer resources (type of compute workers, memory, time of execution) needed to reproduce the experiments?

   Answer: [Yes]

   Justification: We specify the GPU type and batch size used for inference speed evaluation in Section 3, and Section A.3.

   Guidelines:

   - The answer NA means that the paper does not include experiments.
   - The paper should indicate the type of compute workers CPU or GPU, internal cluster, or cloud provider, including relevant memory and storage.
   - The paper should provide the amount of compute required for each of the individual experimental runs as well as estimate the total compute.
   - The paper should disclose whether the full research project required more compute than the experiments reported in the paper (e.g., preliminary or failed experiments that didn't make it into the paper).

9. **Code of ethics**

   Question: Does the research conducted in the paper conform, in every respect, with the NeurIPS Code of Ethics `https://neurips.cc/public/EthicsGuidelines`?

   Answer: [Yes]

   Justification: Our research complies with the NeurIPS Code of Ethics.

   Guidelines:

   - The answer NA means that the authors have not reviewed the NeurIPS Code of Ethics.
   - If the authors answer No, they should explain the special circumstances that require a deviation from the Code of Ethics.
   - The authors should make sure to preserve anonymity (e.g., if there is a special consideration due to laws or regulations in their jurisdiction).

10. **Broader impacts**

    Question: Does the paper discuss both potential positive societal impacts and negative societal impacts of the work performed?

    Answer: [Yes]

    Justification: As a foundational work introducing a lightweight Mamba-based architecture for video action detection, the paper's primary positive impact lies in reducing the computational cost and memory usage as described in Section 1.

    Guidelines:

    - The answer NA means that there is no societal impact of the work performed.
    - If the authors answer NA or No, they should explain why their work has no societal impact or why the paper does not address societal impact.
    - Examples of negative societal impacts include potential malicious or unintended uses (e.g., disinformation, generating fake profiles, surveillance), fairness considerations (e.g., deployment of technologies that could make decisions that unfairly impact specific groups), privacy considerations, and security considerations.

- The conference expects that many papers will be foundational research and not tied to particular applications, let alone deployments. However, if there is a direct path to any negative applications, the authors should point it out. For example, it is legitimate to point out that an improvement in the quality of generative models could be used to generate deepfakes for disinformation. On the other hand, it is not needed to point out that a generic algorithm for optimizing neural networks could enable people to train models that generate Deepfakes faster.
- The authors should consider possible harms that could arise when the technology is being used as intended and functioning correctly, harms that could arise when the technology is being used as intended but gives incorrect results, and harms following from (intentional or unintentional) misuse of the technology.
- If there are negative societal impacts, the authors could also discuss possible mitigation strategies (e.g., gated release of models, providing defenses in addition to attacks, mechanisms for monitoring misuse, mechanisms to monitor how a system learns from feedback over time, improving the efficiency and accessibility of ML).

11. **Safeguards**

    Question: Does the paper describe safeguards that have been put in place for responsible release of data or models that have a high risk for misuse (e.g., pretrained language models, image generators, or scraped datasets)?

    Answer: [NA]

    Justification: Our work does not involve the release of any high-risk models.

    Guidelines:

    - The answer NA means that the paper poses no such risks.
    - Released models that have a high risk for misuse or dual-use should be released with necessary safeguards to allow for controlled use of the model, for example by requiring that users adhere to usage guidelines or restrictions to access the model or implementing safety filters.
    - Datasets that have been scraped from the Internet could pose safety risks. The authors should describe how they avoided releasing unsafe images.
    - We recognize that providing effective safeguards is challenging, and many papers do not require this, but we encourage authors to take this into account and make a best faith effort.

12. **Licenses for existing assets**

    Question: Are the creators or original owners of assets (e.g., code, data, models), used in the paper, properly credited and are the license and terms of use explicitly mentioned and properly respected?

    Answer: [Yes]

    Justification: We properly cite all datasets and pretrained models used in Section 3. All datasets are publicly available and used in accordance with their licenses.

    Guidelines:

    - The answer NA means that the paper does not use existing assets.
    - The authors should cite the original paper that produced the code package or dataset.
    - The authors should state which version of the asset is used and, if possible, include a URL.
    - The name of the license (e.g., CC-BY 4.0) should be included for each asset.
    - For scraped data from a particular source (e.g., website), the copyright and terms of service of that source should be provided.
    - If assets are released, the license, copyright information, and terms of use in the package should be provided. For popular datasets, `paperswithcode.com/datasets` has curated licenses for some datasets. Their licensing guide can help determine the license of a dataset.
    - For existing datasets that are re-packaged, both the original license and the license of the derived asset (if it has changed) should be provided.

- If this information is not available online, the authors are encouraged to reach out to the asset's creators.

13. **New assets**

    Question: Are new assets introduced in the paper well documented and is the documentation provided alongside the assets?

    Answer: [Yes]

    Justification: Algorithms and experiments are well documented in Section 2.

    Guidelines:

    - The answer NA means that the paper does not release new assets.
    - Researchers should communicate the details of the dataset/code/model as part of their submissions via structured templates. This includes details about training, license, limitations, etc.
    - The paper should discuss whether and how consent was obtained from people whose asset is used.
    - At submission time, remember to anonymize your assets (if applicable). You can either create an anonymized URL or include an anonymized zip file.

14. **Crowdsourcing and research with human subjects**

    Question: For crowdsourcing experiments and research with human subjects, does the paper include the full text of instructions given to participants and screenshots, if applicable, as well as details about compensation (if any)?

    Answer: [NA]

    Justification: Our work does not involve crowdsourcing nor research with human subjects.

    Guidelines:

    - The answer NA means that the paper does not involve crowdsourcing nor research with human subjects.
    - Including this information in the supplemental material is fine, but if the main contribution of the paper involves human subjects, then as much detail as possible should be included in the main paper.
    - According to the NeurIPS Code of Ethics, workers involved in data collection, curation, or other labor should be paid at least the minimum wage in the country of the data collector.

15. **Institutional review board (IRB) approvals or equivalent for research with human subjects**

    Question: Does the paper describe potential risks incurred by study participants, whether such risks were disclosed to the subjects, and whether Institutional Review Board (IRB) approvals (or an equivalent approval/review based on the requirements of your country or institution) were obtained?

    Answer: [NA]

    Justification: This study does not involve any human participants or data derived from human subjects, thus IRB approval is not applicable.

    Guidelines:

    - The answer NA means that the paper does not involve crowdsourcing nor research with human subjects.
    - Depending on the country in which research is conducted, IRB approval (or equivalent) may be required for any human subjects research. If you obtained IRB approval, you should clearly state this in the paper.
    - We recognize that the procedures for this may vary significantly between institutions and locations, and we expect authors to adhere to the NeurIPS Code of Ethics and the guidelines for their institution.
    - For initial submissions, do not include any information that would break anonymity (if applicable), such as the institution conducting the review.

16. **Declaration of LLM usage**

Question: Does the paper describe the usage of LLMs if it is an important, original, or non-standard component of the core methods in this research? Note that if the LLM is used only for writing, editing, or formatting purposes and does not impact the core methodology, scientific rigorousness, or originality of the research, declaration is not required.

Answer: [NA]

Justification: Our research does not involve large language models as a core component.

Guidelines:

- The answer NA means that the core method development in this research does not involve LLMs as any important, original, or non-standard components.
- Please refer to our LLM policy (`https://neurips.cc/Conferences/2025/LLM`) for what should or should not be described.

A Technical Appendices and Supplementary Material

A.1 Why Mamba, not Transformers?

We argue that the proposed Mamba-based framework is well-suited for video action detection due to the following reasons:

Linear Complexity. Transformers rely on self-attention to model long-range dependencies, resulting in quadratic complexity with respect to sequence length. Specifically, for a sequence of length L and feature dimension d, the computational cost of self-attention is:

$$\text{Cost}_{\text{Transformer}} = \mathcal{O}(L^2 d). \tag{S1}$$

In contrast, the Mamba block updates hidden states via a linear state space model:

$$\text{Cost}_{\text{Mamba}} = \mathcal{O}(L\, d^2) \approx \mathcal{O}(L). \tag{S2}$$

This is critical for video sequences in real-time or resource-constrained settings.

Causal Modeling. Equation (1) models causal dependencies. Each output depends only on the previous hidden state and current input. This aligns well with the nature of action detection, which relies on the context of preceding and current frames. (However, Mamba may not be well-suited for non-causal tasks such as image restoration, which require access to future tokens.) By contrast, general Transformer-based models perform undifferentiated attention over a large number of previous, current and **future** information tokens, which can introduce redundancy and noise. Mamba, therefore, offers a more efficient and focused modeling paradigm for video-based tasks. This is essentially a coarse-to-fine design. While Transformer attention is detail-oriented (attention), Mamba views the input-output process as a holistic dynamic system. This allows us to design global optimization strategies. From a theoretical perspective, it supports more principled modeling than heuristically stacking attention layers.

However, Mamba lacks explicit attention mechanism. This is why we introduce a minimalistic linear projection (MLP) layer coupled with a purposefully designed loss function to simulate attention-like behavior. This enhancement enables the model to focus on important tokens while preserving the framework performance.

A.2 Related Works

Transformer-Based Action Detection. Recent Transformer-based methods often employ a two-stage pipeline, combining 2D backbones for actor localization with 3D backbones for temporal context extraction. For instance, CycleACR [29] uses a Transformer to model actor-context relations, enhancing detection through cyclic consistency across frames. Query-based approaches like TubeR [3] and WOO [5] build on DETR [2], predicting action tubes and categories with the quadratic complexity of attention mechanisms. In VAT [30], spatiotemporal features are aggregated around actors. Despite these advances, the computational burden of Transformers remains a challenge, especially for long sequences, motivating exploration of efficient alternatives.

Mamba-Related Applications. The Mamba architecture [6], with its linear-time state-space modeling, has emerged as a lightweight alternative to Transformers. VideoMamba [7] adapts Mamba for video classification, achieving competitive top-1 accuracy on K400 by leveraging selective state-space mechanisms to model temporal dependencies efficiently. VideoMambaPro [31] further enhances this by addressing historical decay and element contradiction. MS-Temba [8] extends Mamba to multi-scale temporal localization on datasets like MultiTHUMOS. However, while Mamba excels in classification and localization, its application to video action detection remains underexplored, providing a gap that our MOGO framework addresses with a pure Mamba-based end-to-end solution.

Hybrid Approaches. Mamba has also been explored in hybrid models like MambaVision [32], a work combining Mamba and Transformer for vision tasks, and Simba [33], which augments Mamba with graph networks for skeletal action recognition. Recently, TransMamba [34] introduced a hybrid Transformer-Mamba backbone that adapts attention mechanisms for faster inference while preserving detection accuracy. Similarly, MV-GMN [35] combines rule-based and KNN-based methods with state-space models to enhance robust action recognition.

A.3 Implementation Details

Data Processing. We decode raw videos using the Decord backend and uniformly sample 8 frames for training and evaluation. The input frames are resized and cropped to 224×224 resolution. To construct training and testing samples, we rely on the provided split lists from relative datasets, and retain only clips that have valid annotation files. The underrepresented classes were balanced. For data augmentation during training, we include random short-side scale jittering ([256, 320]), random horizontal flipping, and optional color jittering (PCA-based lighting augmentation). During testing, center cropping is applied after resizing the shorter side to 256. All frames are normalized using the mean and standard deviation values, respectively. Bounding boxes are clipped to image boundaries to avoid numerical instability. Per-frame annotations are matched using the keyframe index of each sampled clip, and annotations are encoded as bounding boxes and class indices for downstream use.

Training Engine. All experiments are conducted using PyTorch with mixed-precision training (torch.cuda.amp.autocast). Gradient clipping is applied to stabilize training. Both the learning rate and weight decay are scheduled using precomputed cosine decay curves and updated at every step. We adopt the AdamW optimizer with betas set to (0.9, 0.999), a weight decay of 0.05, and an initial learning rate of 1e-4. The learning rate is scaled according to the effective batch size and follows a cosine annealing schedule. Training is performed for 50 epochs, with a 5-epoch warmup phase. Since the designed model has an advantage in GPU memory usage, we recommend using a larger batch size for training ($\geq$30). We use a batch size of 30 per GPU and set the update frequency to 1. Training is distributed using torch.distributed, with full synchronization across processes. The total loss consists of a standard object detection loss, including classification, bounding box regression, and GIoU terms, along with a token importance loss. The latter encourages alignment between the model-predicted token importance and the ground-truth spatial token relevance derived from bounding box annotations, computed using binary cross-entropy. (Specifically, we first generate normalized spatial coordinates for all tokens in each frame. Given $H \times W$ spatial patches and T temporal frames, this produces a tensor of shape $[T \times HW, 2]$. These are compared with all bounding boxes to obtain a binary inclusion map.) Evaluation is done using torchmetrics with COCO-style AP. For each sample, we extract predicted logits and bounding boxes, apply softmax to logits, and select the top score per query. Each training batch consists of B video clips, where each clip is represented as a tensor of shape $[3, T, H, W]$. Annotations are processed into lists of dicts with keys *boxes* and *labels*, compatible with TorchMetrics and detection criteria. We log training loss, learning rate, gradient norm, and validation mAP at each step using a custom logger. We use torchrun to launch distributed training with synchronized logging and gradient updates across GPUs.

Model. The core architecture consists of a Mamba-based spatiotemporal encoder and a lightweight decoder. The video encoder is designed based on the Mamba sequence modeling block. Following standard video modeling practices, we adopt a 3D convolutional layer to embed T-frame video clips into patch tokens of shape $[B, T \times N, D]$, where N is the number of spatial patches per frame. Each patch is then projected using a temporal tubelet embedding (kernel size = 1). Spatial and temporal positional embeddings are added separately. The token features are further enhanced by a stack of l_e Mamba-based encoder blocks, each composed of a selective copy mechanism and RMSNorm. To improve efficiency and enable token reduction, we introduce a simple yet effective module that estimates the importance of each token via an MLP. This module predicts a scalar score for each token, and soft masks are applied before the encoder layers. For the decoder, a learnable query embedding of shape $[100, D]$ is provided as input, and an l_d-layer Mamba decoder processes over the encoded memory tokens. The final outputs are passed through a classification head and a bounding box regression head (MLP with sigmoid activation). We adopt RMSNorm as the default normalization layer. The encoder is initialized from a pretrained checkpoint [7] on a large-scale masked video modeling task.

A.4 Ablation Studies - Supplementary

Table S1: **Quantitative ablation (supplementary): experiments results.** (a) Decoder depth. (b) Weights of detection loss. w=w_{cls}: w_{box}: w_{ovl}

(a) Decoder depth.

l_d	1	3	6
mAP	75.6	71.7	32.0

(b) Weights of detection loss.

w	11:1:1	5:1:1	1:1:1	1:5:2	2:3:2
mAP	67.2	68.6	46.3	4.2	35.6

Decoder depth. Table S1(a) shows that a 1-layer decoder gives the best mAP (75.6), while 3 or 6 layers degrade performance, likely due to overfitting. We adopt a single-layer decoder by default. Therefore, MOGO (Mamba Only Glances Once), i.e., our Mamba-based decoder that *glances only once*. For the corresponding training dynamics, please refer to Figure S1.

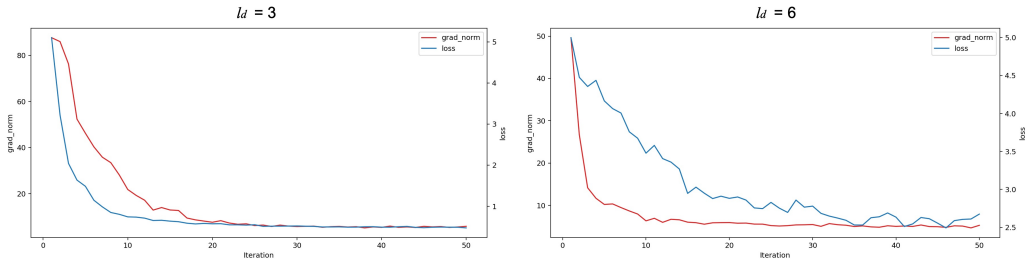

Figure S1: **Training curves and diagnostics.** Training loss (right axis) and gradient norm (left axis) for decoder depths $l_d > 1$.

Weights of detection loss. This set of experiments was conducted with parameter λ (Table 4) fixed. For the detection loss (Table S1(b)), emphasizes the classification weight (w_{cls}) proves beneficial, with ratios of 5:1:1 and 11:1:1 yielding strong mAP scores of 68.6 and 67.2, respectively, compared to lower performance at other settings (e.g., 46.3 at 1:1:1). This suggests that a larger w_{cls} enhances detection accuracy. We note that the 1:5:2 configuration performs poorly; controlled re-runs confirm this trend. When using 1:5:2 weights, we observed high loss (epoch[0]:6.0x/5.9x $\rightarrow$ epoch[29]:2.x) and unstable grad norms (400 after 20 epochs), while mAP stayed under 0.05. In contrast, the 5:1:1 configuration yields stable optimization dynamics: the loss decreases steadily (epoch[0]:8.0x $\rightarrow$ epoch[29]:0.8x), gradient norms consistently drop after 10 epochs, and the mAP rises above 0.6. So now we have enough evidence to say that the 1:5:2 setting may overwhelm optimization with box/ovl weights, preventing the model from learning effective action features.

A.5 Video-level Results

Video-Level Detection mAP. We provide the video-mAP results on JHMDB and UCF101-24 datasets. As shown in Table S2, Table S3 and Table S4, our method achieves lower video-level mAP compared to WOO while outperforming both WOO and TubeR in terms of model size, GFLOPs, and throughput. Because our method detects actions on a designated keyframe within each clip (e.g., the middle frame in an 8-frame snippet), using the remaining frames as temporal context, frame-level metrics such as f-mAP@0.5 are a more appropriate measure. In contrast, video-level mAP emphasizes constructing continuous tubes over the entire clip, which may understate the strengths of our keyframe formulation.

Table S2: **Per-class AP on JHMDB under video-level detection evaluation.** (IoU: 0.2)

Class	brush_hair	catch	clap	climb_stairs	golf	jump	kick_ball	pick	pour	pullup	push
AP	0.833	0.553	0.743	0.725	1.000	0.437	0.791	0.843	1.000	0.937	0.976

Class	run	shoot_ball	shoot_bow	shoot_gun	sit	stand	swing_baseball	throw	walk	wave
AP	0.486	0.450	1.000	0.870	0.297	0.421	0.667	0.181	0.576	0.465

Table S3: **Per-class AP on UCF101-24 under video-level detection evaluation.** (IoU: 0.2)

Class	Basketball	BasketballDunk	Biking	CliffDiving	CricketBowling	Diving	Fencing	FloorGymnastics
AP	0.556	0.519	0.596	0.757	0.404	0.974	0.767	0.981

Class	GolfSwing	HorseRiding	IceDancing	LongJump	PoleVault	RopeClimbing	SalsaSpin	SkateBoarding
AP	0.886	0.940	0.227	0.864	0.928	0.884	0.447	0.993

Class	Skiing	Skijet	SoccerJuggling	Surfing	TennisSwing	TrampolineJumping	VolleyballSpiking	WalkingWithDog
AP	1.000	0.913	0.806	0.596	0.494	0.448	0.189	0.817

Table S4: **Comparison of video-level detection performance and model efficiency.**

Method	Video-mAP@0.2 (U)	Video-mAP@0.2 (J)	Video-mAP@0.5 (U)	Video-mAP@0.5 (J)	#Params	GFLOPs	Throughput
WOO [5]	74.4	70.0	55.8	69.5	314M (head)	252–378	147–176
TubeR (I3D) [3]	**85.3**	**81.8**	**60.2**	**80.7**	-	240	64
Ours	70.8	67.9	39.4	42.0	**82M**	**102–104**	**256**

Video-Level Classification mAP. We further provide the video-level classification mAP results on the JHMDB and UCF101-24 datasets. We conduct this experiment because the dataset provides video-level category labels. Therefore, we aim to evaluate the model's ability to extend frame-level predictions. Our method follows a sliding-window inference strategy to compute video-level predictions. Given an input video, we first extract RGB frames and apply standard preprocessing including resizing, normalization, and batching. The video is divided into clips, and each clip is fed into the model to obtain per-query logits. We compute the average of softmaxed logits (excluding the background class) across all queries and clips. Finally, the class probabilities are aggregated over the video to produce the final prediction. The performance is measured by per-class AP and the overall mean AP. On the JHMDB dataset, as shown in Table S5, our model achieves strong results across most categories, particularly excelling in actions such as *golf*, *pullup*, *push*, and *shoot_bow*. Overall, our approach attains a video-level mAP of 0.812, demonstrating robust performance on this benchmark.

Table S5: **Per-class AP on JHMDB under video-level classification evaluation**.

Class	brush_hair	catch	clap	climb_stairs	golf	jump	kick_ball	pick	pour	pullup	push
AP	0.932	0.711	0.908	0.981	1.000	0.811	0.986	0.870	1.000	1.000	1.000
Class	run	shoot_ball	shoot_bow	shoot_gun	sit	stand	swing_baseball	throw	walk	wave	
AP	0.560	0.555	1.000	0.951	0.378	0.486	0.996	0.560	0.751	0.616	

On the UCF101-24 dataset, it achieves an mAP of 0.971. This result demonstrates that our model possesses strong classification capabilities at the video level without considering bounding box predictions.

Table S6: **Per-class AP on UCF101-24 under video-level classification evaluation**.

Class	Basketball	BasketballDunk	Biking	CliffDiving	CricketBowling	Diving	Fencing	FloorGymnastics
AP	0.927	1.000	0.999	0.993	0.902	1.000	1.000	0.861
Class	GolfSwing	HorseRiding	IceDancing	LongJump	PoleVault	RopeClimbing	SalsaSpin	SkateBoarding
AP	0.929	1.000	1.000	0.993	1.000	1.000	1.000	0.972
Class	Skiing	Skijet	SoccerJuggling	Surfing	TennisSwing	TrampolineJumping	VolleyballSpiking	WalkingWithDog
AP	0.980	0.924	0.851	1.000	0.981	1.000	0.996	0.996

A.6 Result Analysis and Visualization

Per-Class Metric Visualization. To further investigate the importance of keyframe information in our framework, we conduct a study comparing three variants: (1) *Ours*, the full model using both selected tokens and the fixed keyframe segment; (2) *Exchange*, where the keyframe segment is exchanged with non-keyframe tokens; and (3) *Remove*, where the keyframe segment is discarded altogether. As shown in Figure S2, our method consistently outperforms the baselines across most action classes, indicating that preserving keyframe information is crucial for accurate action localization. In particular, categories such as *golf*, *shoot_bow*, and *pullup* benefit significantly from retaining discriminative keyframe cues.

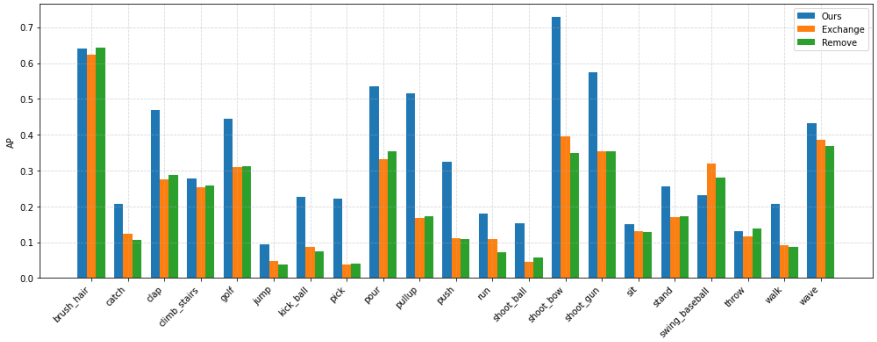

Figure S2: **Per-class AP(0.5:0.95) under different keyframe strategies on the JHMDB dataset.** *Ours* uses both the preserved keyframe and selected tokens. *Exchange* swaps keyframe tokens with other temporal tokens. *Remove* drops keyframe information completely. Preserving keyframe cues leads to the best performance across most categories.

Notably, the impact of certain parameters on mAP may vary slightly across datasets. We ablate the matcher's coefficients to understand the role of classification versus localization in action detection on the UCF101-24 dataset. As shown in Figure S3, using balanced weights (1:1:1) generally yields higher AP across a majority of the 24 classes. Emphasizing classification via (3:1:1) slightly improves a few classes (e.g., *Skiing*).

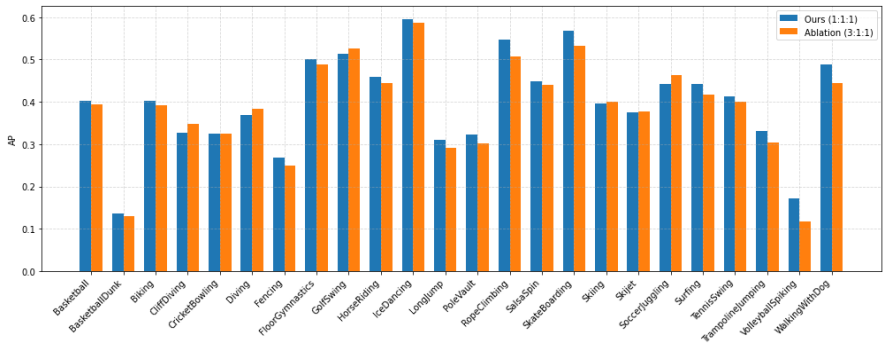

Figure S3: **Per-class AP(0.5:0.95) under different matcher weight ratios on the UCF101-24 dataset.** We compare the decoder performance using the default matcher weights (1:1:1) versus a biased setting (3:1:1).

Learning Token Importance without Explicit Attention. Unlike Transformers, which rely on explicit attention mechanisms to compute token-to-token interactions, Mamba encodes temporal dependencies implicitly through sequential modeling. This makes it challenging to directly interpret token importance. However, token selection is part of our design. As shown in the first rows of Figure S4, raw Mamba outputs tend to produce scattered and less structured token representations. To address this, we propose a heuristic loss function (see Section 2.4), which encourages tokens inside the ground truth bounding boxes to receive higher importance. Furthermore, to avoid introducing significant computational overhead, we insert a lightweight MLP directly before the encoder tokens as shown in Table 1. This MLP outputs a token-wise importance score, which is then multiplied element-wise with the encoder tokens. Notably, the output dimension of the MLP matches the number of encoder tokens, enabling one-to-one correspondence. With this, as shown in the second row, the token activations become more focused on semantically meaningful regions.

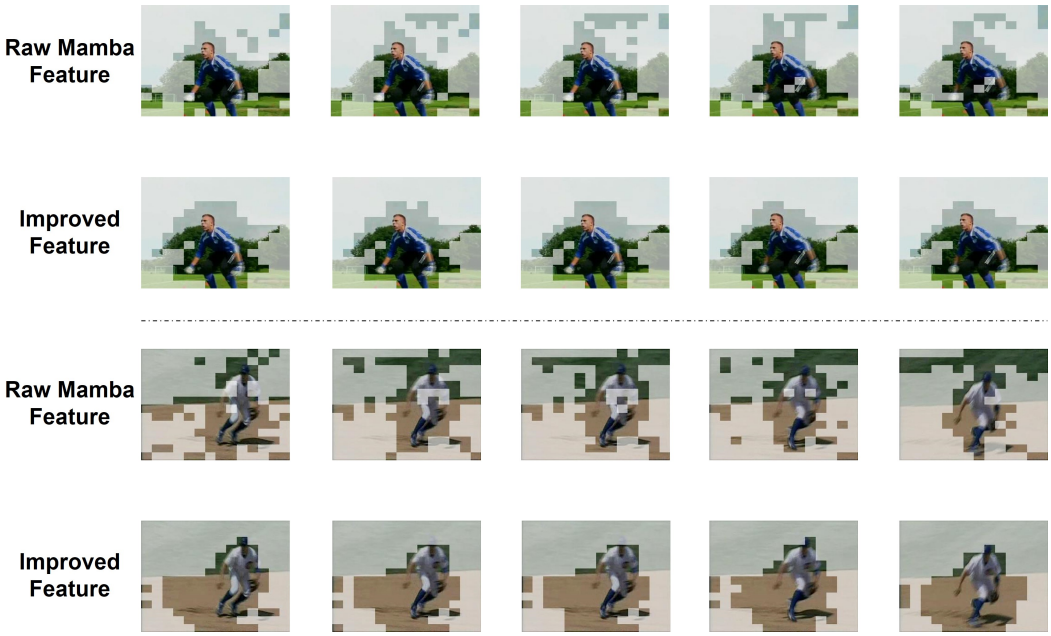

Figure S4: **Visualization of token importance.** Row 1 shows raw Mamba outputs without the loss guidance. Row 2 shows outputs with our proposed importance modeling. Tokens inside target regions are more emphasized.

Spatial Distribution of Preserved Tokens and Corresponding Prediction Results. To better understand the effectiveness of our token selection mechanism and the final prediction results, we visualize the spatial distribution of selected tokens alongside the predicted bounding boxes for some classes as shown in Figure S5. It is evident that the retained tokens are highly concentrated around target subjects and action-relevant regions, showing strong alignment with the predicted bounding boxes. In particular, actions such as *clap* involve fine-grained upper-body motions, where the preserved tokens closely overlap with the hands and head regions. This confirms that our token importance module effectively captures discriminative cues, helping the decoder focus on relevant spatial areas and improving localization precision.

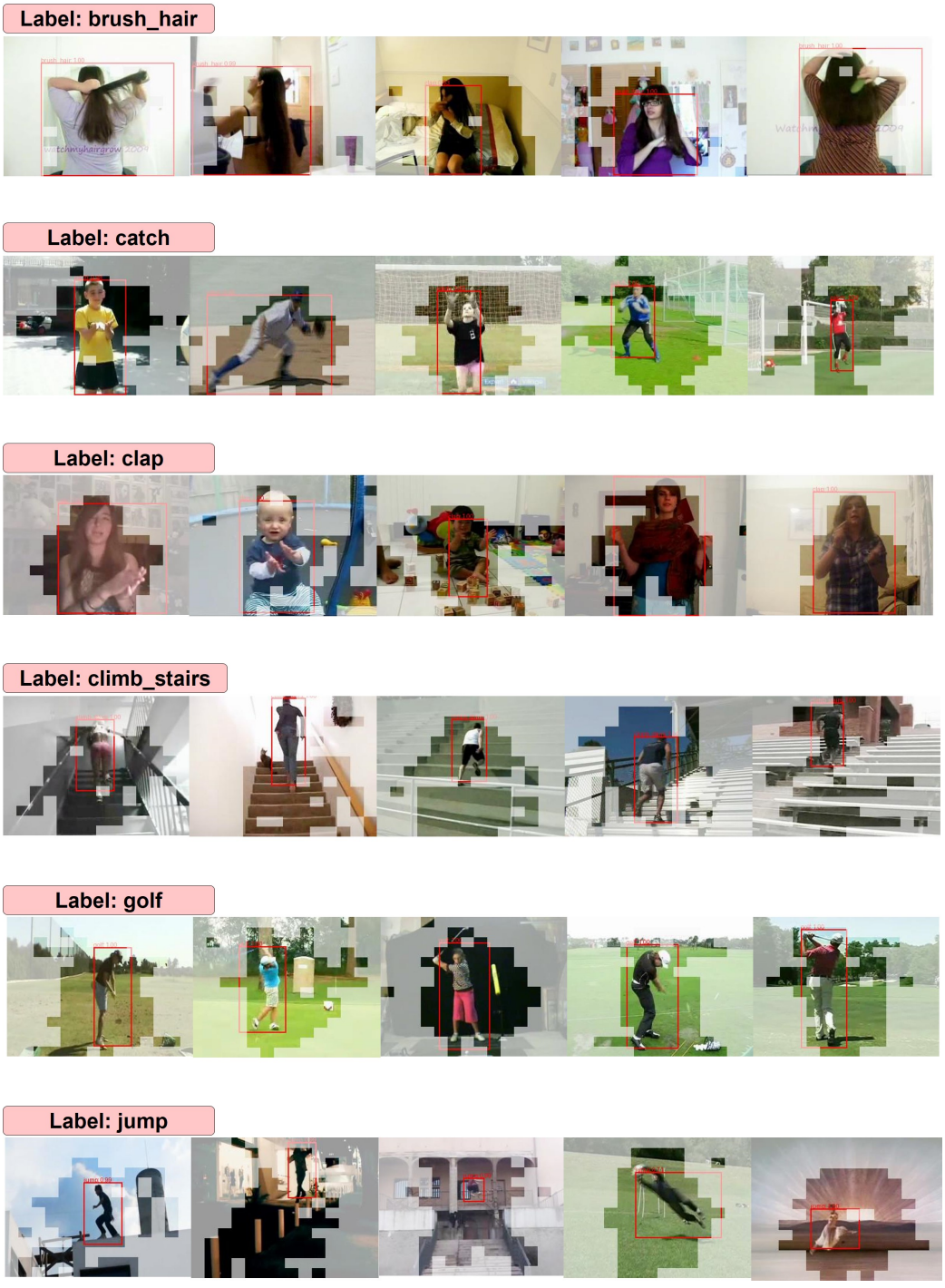

Label: kick_ball

Label: pick

Label: pullup

Label: push

Label: run

Label: shoot_ball

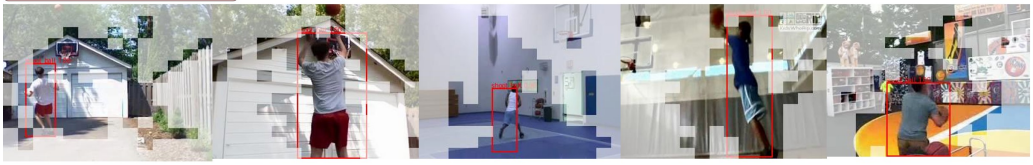

Label: sit

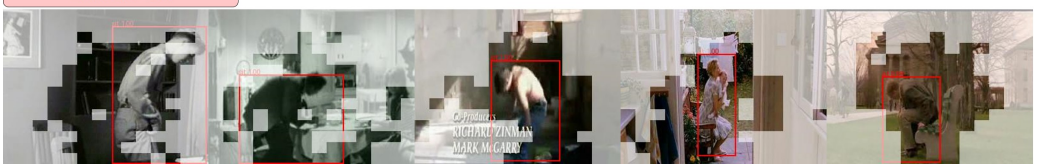

Figure S5: **Visualization of preserved tokens by token importance block on the JHMDB dataset.** Important cues such as people can be effectively retained and are closely related to the bbox prediction of the decoder.

Extension to Multi-Label Detection. On the AVA v2.2 validation set, the adapted MOGO achieved an mAP of 16.2 (at step 26). This demonstrates that MOGO can flexibly extend to multi-label settings with competitive accuracy. Training logs are presented in Figure S6.

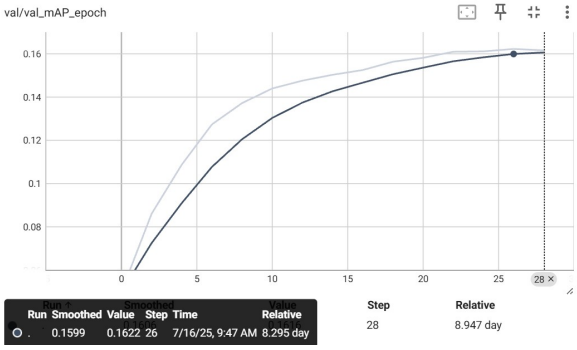

Figure S6: **Training logs on the AVA dataset.**

A.7 Architecture Algorithm

To further clarify our architectural design, we present a step-by-step breakdown of the key modules in the form of pseudocode. Our approach introduces a token importance mechanism into video understanding pipelines, enabling dynamic token weighting and selection for efficient and effective representation learning.

Algorithm 1 Token Importance-Guided Frame Encoding

Require: Video input $x \in \mathbb{R}^{B \times C \times T \times H \times W}$
Ensure: Feature representation f, importance logits s
$x \leftarrow \text{PatchEmbed}(x)$ {Convert frames to patch tokens}
Add spatial positional embedding to each frame
Add temporal positional embedding across frames
$s \leftarrow \text{ImportanceMLP}(x)$ {Predict token importance scores}
$x \leftarrow x \odot \sigma(s)$ {Weight tokens by importance (sigmoid)}
$f \leftarrow \text{MambaEncoder}(x)$
return f, s

Algorithm 2 Top-k Token Selection per Frame

Require: Feature $f \in \mathbb{R}^{B \times N \times D}$, importance $s \in \mathbb{R}^{B \times N}$
Ensure: Reduced feature f_{selected}
Divide f into T temporal segments, each with $N_T = N/T$ tokens
for each frame $t = 1$ to T **do**
    $s_t \leftarrow s[:, t \cdot N_T : (t+1) \cdot N_T]$
    $f_t \leftarrow f[:, t \cdot N_T : (t+1) \cdot N_T, :]$
    Select top-k indices by s_t
    $f'_t \leftarrow$ Gather f_t using top-k indices
    Append f'_t to f_{selected}
end for
return f_{selected}

Algorithm 3 Object Detection with Mamba Decoder

Require: Memory f_{memory}, learnable queries $q \in \mathbb{R}^{Q \times D}$
Ensure: Predicted boxes $\hat{b}$, class logits $\hat{y}$
$q \leftarrow$ Repeat q for each batch and initialize tgt
$hs \leftarrow \text{MambaDecoder}(tgt, f_{\text{memory}})$
$\hat{y} \leftarrow \text{ClassHead}(hs)$ {Predict object class}
$\hat{b} \leftarrow \text{BoxHead}(hs)$ {Predict bounding box (normalized)}
return $\hat{y}, \hat{b}$

Together, these components define the core workflow of our Mamba-based action detection framework.